Received: 13/05/2023
Accepted: 11/08/2023
Published: 15/12/2023

Scientific Journal of Faculty of Science (Menoufia University)
ISSN: 1110-2195

Annular Energy Distribution for a Group of Ions in some Biological and Semi-conductor Materials

El-Sayed Awad*, Fares M. El-kassed, Naira Foda, Ahmed Salah

Physics Department, Faculty of Science, Menoufia University, Shebin El-Koom, Menoufia 32511 Egypt

*Correspondence
Email: ayawad@yahoo.com, awadem704@gmail.com, elsayed_awad@science.menofia.edu.eg (E.M. Awad)

Abstract: Annular energy distribution, AED is a concept deduced from radial dose, RD, that enables estimating the distribution of secondary electrons in a given medium due to ion bombardment. The AED for 337 ions impeded in some distinct targets with biological nature or used in electronic circuits estimated. Gallium arsenide (GaAs), Lithium Niobate (LiNbO3), Pancreas and Thyroid targets investigated for different equal LET groups of ions of the same LET (keV/μm). AED, shell annular energy distribution, SAED, the corresponding maximum annular energy width, rMAEW, and the total annular energy distribution for different targets per nm, TAED for those ions in these different targets determined.

Keywords: Radial dose; Katz radial dose; annular energy distribution; energy distribution at nm scale; LET

1. Introduction

The interaction of radiation with matter has the capability of direct or indirect ionization of atoms and molecules (Nikjoo et al., 2012), Thus, the interaction with spacecraft, satellite parts' body, power production solar cells, and astronauts overspending their period in space, produces secondary electrons (δ-delta rays) that have initial energy above some arbitrary threshold value, Thus, there is a high probability that most of the electrons' power will spread over a wide range

around the ion track (Oda and Lyman, 1967), which decreases the efficiency and the lifetime of the electronic circuits. It may give false estimations of data and information for such devices as solar cells, sensors, and detectors.

Solar cells have been made from varied materials that serve different purposes. It gives the option to increase the Gallium arsenide (GaAs) space cells' efficiencies by up to 26.2 % at some conditions (Algora et al., 2001; Iles, 2000). These cells are applied for space missions that do not strictly require cells with both higher efficiency and better radiation stability (Bailey and Flood, 1998). lithium niobate ($LiNbO_3$) is widely used in integrated and guided-wave optics because of its favorable optical, photorefractive, and thermal properties (Bazzan and Fontana, 2015; Staebler and Amodei, 1972; Weis and Gaylord, 1985) . NASA allows individual programs to set design requirements so that no individual astronaut will exceed their career permissible risk for radiation exposure-induced death from cancer (Snyder, 1997).

Radiation therapy is one of the most widely used therapies for malignancies. The therapeutic use of heavy ions, such as carbon, proton, and helium has gained significant interest due to their advantageous physical and radiobiologic properties as their direct interaction with tumors and to avoid organs at risk of exposure around tumors' locations compared to photon-based therapy. There are currently 13 centers treating patients with carbon ion radiotherapy, with many of these centers publishing promising safety and efficacy data from the first cohort of patients treated (Malouff et al., 2020).

Analytical and numerical methodologies are implemented to estimate ion energy transfer to surrounding media. Ion tracks are composed of a narrow track "core" of a few nanometers in

diameter of severe damage, this core is surrounded by a significantly larger and less damaged (~100 nm) track "halo" (Wang et al., 2022). Monte Carlo, MC simulation codes are used to determine the microscopic energy deposition due to heavy ions in the medium. Geant4-DNA code became the most used code available (Incerti et al., 2014). High-energy ion's radial dose can also be calculated using other MC codes (Fromm et al., 2021) as well.

Radial dose distribution, RDD(r) in the vicinity of ion tracks has many applications, for example, ion-induced modification of materials (Kiefer, 2008) or for estimating the single event upset damage on electronic devices due to heavy ions (Boorboor et al., 2015). Medium radiolysis, damage to DNA by radiation, radiotherapy planning, ion transport software, and estimation of the cell survival rate for heavy particle cancer therapy are other applications based on RDD(r) calculations (Nikjoo et al., 2016). Radial dose distribution, RDD(r) has been calculated analytically using different approaches. Katz's amorphous track model was proposed (Cucinotta et al., 1996; Cucinotta et al., 1999; Katz, 1978; Kobetich and Katz, 1968; Waligórski et al., 2015; Waligórski et al., 1986). In parallel, the local effect model (Chatterjee and Schaefer, 1976), and the classical collision model (Kiefer and Straaten, 1986). Recently, the radial dose distributions were studied by Awad et al (Awad et al., 2022; Awad and Abu-Shady, 2019, 2020; Awad et al., 2018).

Recently it has been updated by introducing the annular dose (AD) concept based on radial dose distribution, RDD (r) (Awad et al., 2022). The annular energy distribution per nanometer, AED, for a given ion was introduced (Awad et al., 2023). This concept exposed the energy distribution around the ion and map the energy distribution at the nanoscale better than the ordinary radial dose.

Tracing and discussing the energy distribution at a nanometer scale around equal LET ions in some distinct targets of biological and electronic circuits interest is the aim of the present work. The concept of AED is deeply discussed by studying 337 ions forming 20 different equal LET groups of ions with a wide energy domain (≈1 to 200 MeV/n) in four different targets. Katz radial dose formula and Butts-Katz range energy (R-E) relation used in the calculation. Annular energy distribution, AED, and shell annular energy distribution, SAED, for these groups were determined. AED peaks at certain shell widths were determined. This width is called the ion's maximum annular energy width, $r_{MAEW,}$ and corresponding to total annular energy distribution, TAED, was determined for all ions under study.

2. Calculations

Secondary electrons produced due to ion bombardment and the spatial distribution of energy deposition are dictated by their number, energy, and corresponding range (Waligórski et al., 1986). The range, R of emitted electrons in a medium is following approximately (Butts and Katz, 1967) the empiric law:

$$R = k\,T/\rho, \tag{1}$$

where R, is in (m), T is the electron energy in (MeV), ρ is the medium density given in (kg/m^3) and the k coefficient results from fitting where $k = 0.1$. The energy transferred to secondary electrons due to the ion hit as a function of the ion's relative velocity, β is expressed as follows:

$$T = \frac{2mc^2\beta^2}{1-\beta^2}, \tag{2}$$

Once T is determined for a given ion, the corresponding range, R, can be obtained from Eq. 1

Radial dose distribution, RDD(r) is the energy deposited per unit mass by a charged particle within a concentric cylindrical shell of infinitesimal thickness, dr at distance r from the ion path and unit length of depth (arbitrary chosen=1 nm), for details please refer to (Spohr, 1990). The RDD formula was suggested by Katz and co-workers (Waligorski et al., 1986) to compute the RDD in (Gy) using the MKS system at any radial distance, r as follows:

$$RDD(r) = N_e \frac{Z^{*2} e^4}{(4\pi\varepsilon_0)^2 \rho m v^2} \frac{1}{\alpha r^2} \left(1 - \frac{r}{R_{eff}}\right)^{\frac{1}{\alpha}}, \quad (3)$$

for T < 1 keV α = 1.079 and for T ≥ 1 keV α = 1.667, ε_0 is the permittivity of free space, ν is the velocity of incident ions. e and m are the electron charge and mass, respectively. N_e is the number of electrons per unit volume of the target and Z^* is the effective charge of the ion according to Barkas' formula (Barkas, 1963); $Z^* = Z(1 - e^{-125\beta Z^{-\frac{2}{3}}})$. The number of electrons per unit volume of the target N_e ($1/m^3$) is not the same for all targets, it is a function of atomic number Z_T, mass number A_T and density of the absorber (Korcyl, 2014; Spohr, 1990).

$$N_e = \frac{\rho Z_T}{A_T} N_A, \quad (4)$$

where Z_T target atomic number, A_T target mass number in (kg/mole), and N_A is Avogadro's number = 6.02×10^{23} (atoms/mole). One can get from the previous Eq. 4, for example, N_e for water target = 3.34×10^{29} ($1/m^3$).

The ion LET is the total energy density around the ion path in 2π directions and it can be determined from the radial dose (Blakely et al., 1984; Cucinotta et al., 1996; Waligórski et al., 2015) as follows:

$$LET = 2\pi \int_{r=R_{min}}^{r=R_{eff}} r\, E(r) dr \quad (5)$$

*w*here E(r) is the radial dose distribution in terms of the energy density distribution (Energy/volume). For the integration, the lower integration limit was always chosen greater than zero to avoid singularity and it was kept at r = 0.1 (nm). The upper integration limit should be adjusted in such a way that the LET calculated by Eq. 5 equals the ion's LET obtained by the SRIM code, (Ziegler et al., 2010). Thus, the effective range, R_{eff} was obtained.

To trace the distribution of energy per nm around the ion path, the annular energy distribution, AED is introduced (Awad et al., 2023), it gives the energy distribution at any point around the ion trajectory over 2π directions. The total AED is the ion's LET. Thus, AED is the detailed annular energy distribution delivered by the secondary electron at the nanometer scale around the ion trajectory over 2π directions. AED in $\frac{J}{m}$ using the MKS system can be defined (Spohr, 1990) in terms of the energy density E(r) and details of ions and target parameters as follows:

$$AED\left(\frac{J}{m}\right) = 2\pi N_e \frac{Z^{*2} e^4}{(4\pi\varepsilon_0)^2\, m v^2 \alpha^2} \int_{R=R_{min}}^{R=R_{eff}} \int_{r=0.1}^{r=R_{min}} \frac{1}{R^2} \left(1 - \frac{r}{R}\right)^{\left(\frac{1}{\alpha}-1\right)} dr\, dR \quad (6)$$

AED is easily converted to $\frac{eV}{nm}$ and it depends on the shell width, R_{min}. For AED calculation, starting limit was chosen at r = 0.1 nm, and the final limit was chosen at r = R_{eff}(nm) and is kept fixed throughout the whole calculation. AED at any position or width is thus controlled by choosing r = R_{min} (nm) and the distance between r = 0.1(nm) to r = R_{min}(nm) is called the annular energy width, AEW. R_{min} is thus controlling the width and you change every time, and you can compute AED for each nanometer or more as you wish. Thus, R_{min} is varying from r = 0.1 nm to r = R_{eff}(nm). AED integrates (summed up) the radial energy for many shells around the ions. When AED is plotted as a function of the annular energy-dose width $r = 0.1(nm) \longrightarrow R_{min}(nm)$ a peak is found. This peak is at a certain radius called the maximum annular energy width, r_{MAEW}. The code written for Eq. 6 with consideration of the N_e in Eq. 4 for the various targets, enables these calculations. An algorithm was constructed to calculate the above integration numerically by using the *Mid-Point Method* of integration using Fortran and Python programming languages. The shell annular energy distribution, SAED, is determined by subtracting two annular energies of width 1 nm of two successive annular widths (1 nm apart). Simply, subtract the n^{th} annular energy of width 1 nm from the $(n+1)^{th}$ annular energy of width 1 nm which allows a difference between those two energies.

3. Linear Energy Transfer, LET groups

337 ions bombarded in different targets are having biological nature and electronic circuits components. Gallium arsenide (GaAs), Lithium Niobate ($LiNbO_3$), Pancreas and Thyroid targets were studied. Twenty (20) different equal LET groups at 25, 65.05, 150, 500, and 1000 keV/μm,

were composed in different targets, and SRIM code is used. Examples of some groups are given in different targets in Tables 1-4. Ion's energy is widely studied from ≈ 1 to 200 MeV/n. The electronic energy loss at the surface of the foil LET_{SRIM} (keV/μm) is considered only.

Table 1. Groups details for gallium arsenide target.

Group	LET (KeV/μm)	Ion	E/n (MeV/n)	β	Z*	R (Butts-Kattz) nm	R(eff) nm	Maximum Annular Energy Width (r_{MAEW}) (nm)	Total Annular Energy Distribution (TAED) (eV/nm)
G-1	25	1 H 1	4.3	0.1	1	176	173.6	109	115.8
		2 He 4	28.9	0.2	2	1212	1173.1	733	70.9
		3 Li 7	85.5	0.4	3	3691	3527.1	2205	58.8
		4 Be 9	187	0.6	4	8491	8064.1	5040	54.9
G-2	65.05	2 He 4	8	0.1	2	330	323.8	202	248.9
		3 Li 7	24	0.2	3	1004	973.9	609	190.8
		4 Be 9	49.2	0.3	4	2086	2011.1	1257	172
		5 B 11	89.8	0.4	5	3886	3720.1	2325	156.5
		6 C 12	152.5	0.5	6	6810	6476.1	4048	144.8
		7 N 14	256.4	0.6	7	12036	11354.1	7097	133.9
G-3	150	2 He 4	2.3	0.1	2	95	94.1	59	850.1
		3 Li 7	7.8	0.1	3	323	316.9	198	573
		4 Be 9	15.5	0.2	4	644	629.6	394	519.5
		5 B 11	29.6	0.2	5	1243	1205.1	753	433.3
		6 C 12	48.3	0.3	6	2046	1971.1	1232	393.7
		7 N 14	74.6	0.4	7	3200	3064.1	1915	361.3
		8 O 16	107.4	0.4	8	4686	4468.1	2793	343.5
		9 F 19	150.7	0.5	9	6723	6384.1	3990	328.9

		10 Ne 20	207.6	0.6	10	9519	9007.1	5630	317.8
G-4	500	3 Li 7	1.1	0	2.8	44	43.7	27	3650.4
		4 Be 9	3.1	0.1	3.9	130	128.4	80	2420.7
		5 B 11	5.8	0.1	5	239	235.2	147	2104.4
		6 C 12	9.3	0.1	6	386	378.7	237	1904.2
		7 N 14	14.3	0.2	7	594	580.4	363	1711.1
		8 O 16	21.1	0.2	8	879	854.7	534	1535.8
		9 F 19	29.3	0.2	9	1227	1188.1	743	1417.7
		10 Ne 20	38.7	0.3	10	1628	1571.1	982	1345.7
		11 Na 23	51.3	0.3	11	2176	2089.1	1306	1251.4
		12 Mg 24	61.9	0.3	12	2640	2535.6	1585	1254.1
		13 Al 27	82.3	0.4	13	3548	3381.1	2113	1140.9
		14 Si 28	96.3	0.4	14	4177	3985.1	2491	1155.4
		15 P 31	117.9	0.5	15	5173	4921.1	3076	1116.6
		16 S 32	147.8	0.5	16	6584	6228.1	3893	1056
		17 Cl 35	169.8	0.5	17	7647	7243.1	4527	1068.6
		18 Ar 40	213.7	0.6	18	9831	9252.1	5783	1007.8
G-5	1000	5 B 11	1.8	0.1	4.6	73	72.4	45	5988.8
		6 C 12	3.3	0.1	5.8	137	135.3	85	4909.3
		7 N 14	5.4	0.1	6.8	223	219.5	137	4264

		8 O 16	7.7	0.1	7.9	318	312.4	195	3979.7
		9 F 19	10.8	0.2	8.9	447	437.9	274	3653.6
		10 Ne 20	14.3	0.2	9.9	554	542.8	339	3672.6
		11 Na 23	18.7	0.2	10.9	780	760.1	475	3218.9
		12 Mg 24	23.7	0.2	11.9	992	964.3	603	3056.5
		13 Al 27	31.8	0.3	13	1335	1289.3	806	2721.7
		14 Si 28	37.9	0.3	14	1594	1538	961	2679.4
		15 P 31	45.7	0.3	15	1934	1861.1	1163	2579.2
		16 S 32	55.1	0.3	16	2341	2246.1	1404	2474.1
		17 Cl 35	63.6	0.4	17	2713	2601.1	1626	2452.7
		18 Ar 40	77.2	0.4	18	3317	3165.1	1978	2313.1
		19 K 39	83.5	0.4	19	3598	3444.5	2153	2404.8
		20 Ca 40	97.5	0.4	20	4232	4041.1	2526	2329.5
		21 Sc 45	110.5	0.4	21	4829	4607.1	2880	2308.6
		22 Ti 48	125.9	0.5	22	5547	5285.1	3303	2271.6
		23 V 51	144.8	0.5	23	6440	6121.1	3826	2216.3

		24 Cr 52	165.1	0.5	24	7416	7036.1	4398	2175.5
		25 Mn 55	184.5	0.6	25	8370	7938.1	4962	2166.9
		26 Fe 56	208.8	0.6	26	9579	9073.1	5671	2138.2

Table 2. Groups details for lithium niobate target.

Group	LET (KeV/μm)	Ion	E/n (MeV/n)	β	Z*	R (Butts-Kattz) nm	R(eff) nm	Maximum Annular Energy Width (r_{MAEW}) (nm)	Total Annular Energy Distribution (TAED) (eV/nm)
G-1	25	1 H 1	4.0	0.1	1.0	206.0	202.6	127.0	25.0
		2 He 4	51.4	0.2	2.0	1,329.0	1,282.1	801.0	25.0
		3 Li 7	173.1	0.4	3.0	3,937.0	3,746.1	2,342.0	25.0
		4 Be 9	354.4	0.5	4.0	8,717.0	8,245.1	5,154.0	25.0
		5 B 11	732.0	0.7	5.0	20,012.0	18,740.1	11,713.0	25.0
G-2	65.05	2 He 4	7.3	0.1	2.0	376.0	367.7	230.0	65.0
		3 Li 7	21.4	0.2	3.0	1,105.0	1,068.1	668.0	64.9
		4 Be 9	43.3	0.3	4.0	2,261.0	2,171.4	1,357.0	65.1
		5 B 11	78.0	0.4	5.0	4,147.0	3,953.5	2,471.0	65.0
		6 C 12	129.7	0.5	6.0	7,077.0	6,702.1	4,189.0	65.0
		7 N 14	211.6	0.6	7.0	12,027.0	11,296.1	7,061.0	65.1
		8 O 16	338.4	0.7	8.0	20,408.0	19,043.1	11,903.0	65.1

G-3	150	2 He 4	2.3	0.1	2.0	116.0	114.5	72.0	150.0
		3 Li 7	3.5	0.1	3.0	181.0	179.8	112.0	150.2
		4 Be 9	15.0	0.2	4.0	773.0	750.7	469.0	150.0
		5 B 11	26.3	0.2	5.0	1,360.0	1,313.1	821.0	150.9
		6 C 12	42.5	0.3	6.0	2,220.0	2,131.1	1,332.0	149.6
		7 N 14	64.9	0.4	7.0	3,427.0	3,267.7	2,043.0	150.0
		8 O 16	92.5	0.4	8.0	4,955.0	4,704.1	2,940.0	150.0
		9 F 19	128.4	0.5	9.0	7,002.0	6,619.1	4,137.0	150.1
		10 Ne 20	173.5	0.5	10.0	9,678.0	9,119.1	5,700.0	150.1
		11 Na 23	246.1	0.6	11.0	14,217.0	13,287.5	8,305.0	150.0
G-4	500	3 Li 7	1.2	0.1	2.9	60.0	59.4	37.0	499.1
		4 Be 9	2.9	0.1	3.9	149.0	146.8	92.0	499.5
		5 B 11	5.4	0.1	4.9	278.0	272.6	170.0	499.9
		6 C 12	9.0	0.1	6.0	462.0	450.8	282.0	500.0
		7 N 14	13.9	0.2	7.0	716.0	694.7	434.0	500.0
		8 O 16	19.8	0.2	8.0	1,021.0	986.5	617.0	500.0
		9 F 19	25.9	0.2	9.0	1,340.0	1,292.8	808.0	500.0
		10 Ne 20	34.1	0.3	10.0	1,771.0	1,702.8	1,064.0	500.0
		11 Na 23	45.1	0.3	11.0	2,356.0	2,252.9	1,408.0	500.0
		12 Mg 24	54.1	0.3	12.0	2,841.0	2,718.1	1,699.0	499.4

		13 Al 27	71.3	0.4	13.0	3,780.0	3,587.1	2,242.0	499.9
		14 Si 28	83.2	0.4	14.0	4,437.0	4,215.1	2,635.0	500.2
		15 P 31	101.2	0.4	15.0	5,447.0	5,158.1	3,224.0	500.2
		16 S 32	125.2	0.5	16.0	6,816.0	6,420.1	4,013.0	500.2
		17 Cl 35	143.6	0.5	17.0	7,891.0	7,441.1	4,651.0	499.8
		18 Ar 40	178.3	0.5	18.0	9,966.0	9,336.1	5,836.0	499.8
		19 K 39	195.5	0.6	19.0	11,024.0	10,374.1	6,484.0	500.2
		20 Ca 40	233.8	0.6	20.0	13,425.0	12,592.1	7,871.0	500.0
G-5		5 B 11	1.7	0.1	4.6	87.0	86.0	54.0	1,000.2
		6 C 12	3.0	0.1	5.7	156.0	153.7	96.0	999.1
		7 N 14	5.0	0.1	6.8	256.0	251.2	157.0	1,000.2
		8 O 16	7.3	0.1	7.8	375.0	366.7	229.0	1,000.2
		9 F 19	10.5	0.1	8.9	537.0	522.8	327.0	1,000.1
	1000	10 Ne 20	13.9	0.2	9.9	716.0	694.9	434.0	1,000.0
		11 Na 23	17.8	0.2	10.9	916.0	886.9	554.0	999.9
		12 Mg 24	21.9	0.2	11.9	1,129.0	1,091.7	682.0	1,000.0
		13 Al 27	27.7	0.2	12.9	1,435.0	1,381.9	864.0	1,000.0

		14 Si 28	33.3	0.3	13.9	1,731.0	1,663.9	1,040.0	1,000.0
		15 P 31	40.2	0.3	15.0	2,097.0	2,010.1	1,256.0	999.0
		16 S 32	48.1	0.3	16.0	2,516.0	2,404.1	1,503.0	1,002.2
		17 Cl 35	55.5	0.3	17.0	2,917.0	2,785.1	1,741.0	1,000.7
		18 Ar 40	67.0	0.4	18.0	3,542.0	3,365.1	2,103.0	999.8
		19 K 39	72.4	0.4	19.0	3,840.0	3,661.1	2,288.0	999.3
		20 Ca 40	84.1	0.4	20.0	4,487.0	4,266.1	2,667.0	1,000.5
		21 Sc 45	95.2	0.4	21.0	5,105.0	4,849.1	3,031.0	1,000.8
		22 Ti 48	107.9	0.4	22.0	5,826.0	5,527.1	3,455.0	999.4
		23 V 51	122.9	0.5	23.0	6,688.0	6,332.1	3,958.0	999.3
		24 Cr 52	139.7	0.5	24.0	7,664.0	7,241.1	4,526.0	999.6
		25 Mn 55	155.5	0.5	25.0	8,595.0	8,117.1	5,074.0	1,000.3
		26 Fe 56	174.5	0.5	26.0	9,737.0	9,184.1	5,741.0	999.9
		27 Co 59	195.1	0.6	27.0	10,998.0	10,363.1	6,477.0	999.8
		28 Ni 58	222.2	0.6	28.0	12,694.0	11,929.1	7,456.0	999.8

Table 3. Groups details for pancreas target.

Group	LET (KeV /µm)	Ion	E/n (MeV/n)	β	Z*	R (Butts-Kattz) nm	R(eff) nm	Maximum Annular Energy Width (r_{MAEW}) (nm)	Total Annular Energy Distribution (TAED) (eV/nm)
G-1	25	1 H 1	1.2	0.0	1.0	241.0	237.1	148.0	104.5
		2 He 4	7.4	0.1	2.0	1547.0	1491.1	932.0	66.3
		3 Li 7	20.0	0.2	3.0	4231.0	4026.1	2517.0	56.0
		4 Be 9	39.2	0.3	4.0	8364.0	7906.1	4942.0	52.4
		5 B 11	68.9	0.4	5.0	14929.0	13993.2	8746.0	48.8
		6 C 12	111.7	0.5	6.0	24735.0	23009.8	14382.0	46.1
		7 N 14	176.7	0.5	7.0	40433.0	37254.9	23286.0	43.3
		8 O 16	270.8	0.6	8.0	64822.0	59290.7	37060.0	41.5
G-2	65.05	2 He 4	2.2	0.1	2.0	456.0	445.4	278.0	220.5
		3 Li 7	6.2	0.1	3.0	1305.0	1259.9	788.0	176.1
		4 Be 9	12.8	0.2	4.0	2696.0	2577.5	1611.0	153.9
		5 B 11	21.0	0.2	5.0	4435.0	4227.7	2643.0	148.7
		6 C 12	33.2	0.3	6.0	7065.0	6686.1	4179.0	138.0
		7 N 14	49.6	0.3	7.0	10651.0	10002.1	6252.0	128.8
		8 O 16	69.3	0.4	8.0	15024.0	14043.1	8778.0	124.1
		9 F 19	94.0	0.4	9.0	20632.0	19198.1	12000.0	120.1
		10 Ne 20	124.0	0.5	10.0	27644.0	25632.1	16021.0	117.2

		11 Na 23	169.2	0.5	11.0	38565.0	35421.1	22140.0	110.6
		12 Mg 24	209.6	0.6	12.0	48737.0	44858.1	28038.0	111.9
		13 Al 27	304.6	0.7	13.0	74072.0	66899.1	41815.0	101.4
G-3	150	2 He 4	0.6	0.0	1.9	132.0	130.2	81.0	682.0
		3 Li 7	2.1	0.1	2.9	442.0	431.3	270.0	497.9
		4 Be 9	4.7	0.1	4.0	984.0	950.1	594.0	409.1
		5 B 11	8.1	0.1	5.0	1694.0	1627.1	1017.0	376.1
		6 C 12	12.5	0.2	6.0	2628.0	2512.1	1570.0	353.7
		7 N 14	18.0	0.2	7.0	3795.0	3613.1	2258.0	337.8
		8 O 16	24.6	0.2	8.0	5210.0	4943.1	3090.0	326.1
		9 F 19	32.8	0.3	9.0	6984.0	6599.1	4125.0	313.3
		10 Ne 20	42.4	0.3	10.0	9052.0	8526.1	5329.0	304.5
		11 Na 23	55.3	0.3	11.0	11901.0	11132.1	6958.0	287.8
		12 Mg 24	66.1	0.4	12.0	14314.0	13408.1	8381.0	291.1
		13 Al 27	87.1	0.4	13.0	19056.0	17642.1	11027.0	267.7
		14 Si 28	101.0	0.4	14.0	22260.0	20671.1	12920.0	273.1
		15 P 31	122.7	0.5	15.0	27341.0	25288.1	15806.0	266.0
		16 S 32	152.8	0.5	16.0	34555.0	31702.1	19815.0	253.3
		17 Cl 35	174.9	0.5	17.0	39972.0	36773.1	22985.0	257.4
		18 Ar 40	218.3	0.6	18.0	50954.0	46442.1	29029.0	244.5

G-4	500	5 B 11	1.5	0.1	4.5	305.0	298.0	186.0	1711.3
		6 C 12	2.4	0.1	5.6	508.0	494.5	309.0	1569.4
		7 N 14	3.7	0.1	6.7	779.0	755.2	472.0	1450.8
		8 O 16	5.2	0.1	7.7	1097.0	1060.5	663.0	1381.2
		9 F 19	7.6	0.1	8.8	1586.0	1522.1	951.0	1243.8
		10 Ne 20	9.9	0.1	9.8	2080.0	1989.1	1243.0	1188.6
		11 Na 23	12.1	0.2	10.8	2546.0	2435.1	1522.0	1188.6
		12 Mg 24	14.8	0.2	11.8	3114.0	2974.1	1859.0	1168.2
		13 Al 27	18.0	0.2	12.8	3796.0	3617.1	2261.0	1137.8
		14 Si 28	21.0	0.2	13.8	4437.0	4228.1	2643.0	1139.9
		15 P 31	25.3	0.2	14.9	5369.0	5098.1	3187.0	1096.3
		16 S 32	30.2	0.2	15.9	6413.0	6068.1	3793.0	1058.1
		17 Cl 35	35.2	0.3	16.9	7501.0	7080.1	4425.0	1034.1
		18 Ar 40	42.2	0.3	17.9	9010.0	8452.1	5283.0	981.6
		19 K 39	45.5	0.3	18.9	9744.0	9181.1	5739.0	1018.2
		20 Ca 40	52.6	0.3	19.9	11308.0	10617.1	6636.0	988.4
		21 Sc 45	58.9	0.3	20.9	12701.0	11918.1	7449.0	983.6

		22 Ti 48	66.2	0.4	21.9	14320.0	13418.1	8387.0	972.2
		23 V 51	74.5	0.4	22.9	16198.0	15144.1	9466.0	956.0
		24 Cr 52	83.7	0.4	23.9	18280.0	17053.1	10659.0	940.1
		25 Mn 55	92.0	0.4	24.9	20172.0	18817.1	11762.0	939.8
		26 Fe 56	102.0	0.4	25.9	22483.0	20943.1	13090.0	930.2
		27 Co 59	112.3	0.5	26.9	24889.0	23165.1	14479.0	924.7
		28 Ni 58	126.1	0.5	28	28133.0	26097.1	16312.0	903.9
		29 Cu 63	138.5	0.5	29.0	31105.0	28826.1	18018.0	897.9
		30 Zn 64	152.7	0.5	30.0	34536.0	31954.1	19973.0	888.7
		31 Ga 69	167.0	0.5	31.0	38036.0	35168.1	21982.0	884.7
		32 Ge 74	183.1	0.5	32.0	42027.0	38814.1	24261.0	878.5
		33 As 75	200.9	0.6	33.0	46503.0	42895.1	26811.0	871.7
		34 Se 80	221.4	0.6	34.0	51777.0	47668.1	29795.0	861.7
		35 Br 79	243.3	0.6	35.0	57483.0	52844.1	33030.0	854.3
G-5	1000	7 N 14	0.2	0.0	3.5	40.0	39.8	25.0	7693.5
		8 O 16	1.5	0.1	6.6	304.0	297.7	186.0	3629.9
		9 F 19	2.2	0.1	7.7	453.0	442.3	276.0	3354.7
		10 Ne 20	3.2	0.1	8.9	665.0	646.2	404.0	3035.8
		11 Na 23	3.9	0.1	9.9	820.0	797.0	498.0	3045.6

		12 Mg 24	5.2	0.1	11.0	1080.0	1046.3	654.0	2865.6
		13 Al 27	6.6	0.1	12.1	1386.0	1338.1	836.0	2706.9
		14 Si 28	8.1	0.1	13.2	1709.0	1645.9	1029.0	2606.7
		15 P 31	9.9	0.1	14.2	2086.0	2003.1	1252.0	2502.9
		16 S 32	11.9	0.2	15.3	2512.0	2405.3	1503.0	2411.2
		17 Cl 35	13.9	0.2	16.3	2933.0	2804.1	1753.0	2364.8
		18 Ar 40	16.4	0.2	17.4	3447.0	3286.3	2054.0	2289.8
		19 K 39	17.8	0.2	18.4	3746.0	3580.1	2238.0	2357.1
		20 Ca 40	20.4	0.2	19.4	4299.0	4101.1	2563.0	2304.1
		21 Sc 45	22.7	0.2	20.4	4795.0	4573.1	2858.0	2298.5
		22 Ti 48	25.5	0.2	21.4	5406.0	5148.1	3218.0	2262.9
		23 V 51	29.2	0.2	22.5	6197.0	5883.1	3677.0	2187.7
		24 Cr 52	32.9	0.3	23.5	6994.0	6624.1	4140.0	2138.2
		25 Mn 55	36.1	0.3	24.5	7696.0	7286.1	4554.0	2128.1
		26 Fe 56	39.9	0.3	25.5	8512.0	8048.1	5030.0	2103.5

		27 Co 59	43.8	0.3	26.6	9372.0	8852.1	5533.0	2082.2
		28 Ni 58	48.7	0.3	27.6	10434.0	9832.1	6146.0	2037.9
		29 Cu 63	53.0	0.3	28.6	11395.0	10729.1	6706.0	2024.5
		30 Zn 64	58.2	0.3	29.6	12533.0	11780.1	7363.0	1995.2
		31 Ga 69	63.2	0.4	30.6	13660.0	12826.1	8017.0	1977.8
		32 Ge 74	68.4	0.4	31.6	14826.0	13910.1	8695.0	1964.6
		33 As 75	74.3	0.4	32.7	16154.0	15135.1	9460.0	1943.5
		34 Se 80	80.6	0.4	33.7	17578.0	16447.1	10280.0	1922.9
		35 Br 79	87.2	0.4	34.7	19077.0	17827.1	11143.0	1904.5
		36 Kr 84	96.2	0.4	35.7	21145.0	19686.1	12305.0	1853.2
		37 Rb 85	102.9	0.4	36.7	22688.0	21117.1	13199.0	1849.9
		38 Sr 88	110.2	0.4	37.7	24393.0	22690.1	14182.0	1841.9
		39 Y 89	119.0	0.5	38.7	26468.0	24579.1	15363.0	1820.6
		40 Zr 90	129.1	0.5	39.8	28852.0	26730.1	16708.0	1792.6
		41 Nb 93	136.9	0.5	40.8	30708.0	28460.1	17789.0	1796.8
		42 Mo 98	149.1	0.5	41.8	33648.0	31091.1	19433.0	1762.3
		43 Tc 97	160.0	0.5	42.8	36309.0	33505.1	20942.0	1747.7
		44 Ru 102	170.8	0.5	43.8	38963.0	35927.1	22456.0	1739.6
		45 Rh 103	186.0	0.6	44.8	42756.0	39294.1	24561.0	1705.7
		46 Pd 106	196.2	0.6	45.8	45327.0	41686.1	26056.0	1712.6

Table 4. Groups details for thyroid target.

Group	LET (KeV /µm)	Ion	E/n (MeV/n)	β	Z*	R (Butts-Kattz) nm	R(eff) nm	Maximum Annular Energy Width (r_{MAEW}) (nm)	Total Annular Energy Distribution (TAED) (eV/nm)
G-1	25	1 H 1	1.1	0.0	1.0	237.0	233.2	146.0	105.9
		2 He 4	7.3	0.1	2.0	1539.0	1484.1	928.0	66.5
		3 Li 7	19.9	0.2	3.0	4212.0	4008.1	2505.0	56.1
		4 Be 9	39.0	0.3	4.0	8328.0	7874.1	4922.0	52.6
		5 B 11	68.6	0.4	5.0	14866.0	13937.1	8711.0	48.8
		6 C 12	111.2	0.4	6.0	24618.0	22907.1	14318.0	46.2
		7 N 14	176.0	0.5	7.0	40256.0	37099.1	23189.0	43.3
		8 O 16	269.4	0.6	8.0	64434.0	58955.1	36850.0	41.6
G-2	65.05	2 He 4	2.2	0.1	2.0	452.0	441.6	276.0	222.0
		3 Li 7	6.2	0.1	3.0	1298.0	1253.4	783.0	176.6
		4 Be 9	12.8	0.2	4.0	2689.0	2570.9	1607.0	153.9
		5 B 11	20.9	0.2	5.0	4414.0	4208.6	2631.0	149.1
		6 C 12	32.5	0.3	6.0	6909.0	6551.1	4095.0	140.6
		7 N 14	49.5	0.3	7.0	10608.0	9964.1	6228.0	129.0
		8 O 16	69.0	0.4	8.0	14957.0	13983.1	8740.0	124.3
		9 F 19	93.6	0.4	9.0	20545.0	19121.1	11952.0	120.3
		10 Ne 20	123.6	0.5	10.0	27532.0	25532.1	15959.0	117.4
		11 Na 23	168.4	0.5	11.0	38382.0	35262.1	22041.0	110.7
		12 Mg 24	208.5	0.6	12.0	48460.0	44617.1	27888.0	112.1
		13 Al 27	303.0	0.7	13.0	73610.0	66507.1	41570.0	101.6
G-3	150	3 Li 7	2.1	0.1	2.9	439.0	428.5	268.0	500.2
		4 Be 9	4.7	0.1	4.0	980.0	946.7	592.0	409.5
		5 B 11	8.1	0.1	5.0	1691.0	1624.1	1015.0	375.9
		6 C 12	12.5	0.2	6.0	2625.0	2509.1	1568.0	353.5
		7 N 14	17.9	0.2	7.0	3784.0	3602.1	2252.0	337.8
		8 O 16	24.5	0.2	8.0	5193.0	4927.1	3080.0	326.3
		9 F 19	32.8	0.3	9.0	6966.0	6582.1	4114.0	313.6
		10 Ne 20	42.2	0.3	10.0	9020.0	8497.1	5311.0	305.0

		11 Na 23	55.2	0.3	11.0	11875.0	11108.1	6943.0	288.0
		12 Mg 24	66.0	0.4	12.0	14278.0	13375.1	8360.0	291.2
		13 Al 27	86.9	0.4	13.0	19005.0	17595.1	10998.0	267.7
		14 Si 28	100.7	0.4	14.0	22185.0	20604.1	12879.0	273.3
		15 P 31	122.4	0.5	15.0	27249.0	25206.1	15755.0	266.2
		16 S 32	152.3	0.5	16.0	34441.0	31602.1	19753.0	253.5
		17 Cl 35	174.3	0.5	17.0	39830.0	36646.1	22906.0	257.6
		18 Ar 40	217.5	0.6	18.0	50760.0	46270.1	28921.0	244.6
G-4		6 C 12	2.4	0.1	5.6	502.0	488.8	306.0	1581.8
		7 N 14	3.7	0.1	6.7	772.0	748.7	468.0	1459.4
		8 O 16	5.2	0.1	7.7	1089.0	1053.0	658.0	1387.1
		9 F 19	7.5	0.1	8.8	1580.0	1516.7	948.0	1245.3
		10 Ne 20	9.9	0.1	9.8	2075.0	1984.8	1241.0	1190.0
		11 Na 23	12.1	0.2	10.8	2539.0	2428.4	1518.0	1188.6
		12 Mg 24	14.7	0.2	11.8	3104.0	2964.8	1853.0	1169.7
		13 Al 27	17.9	0.2	12.8	3781.0	3603.1	2252.0	1140.1
		14 Si 28	20.9	0.2	13.8	4417.0	4210.1	2632.0	1142.9
		15 P 31	25.2	0.2	14.9	5339.0	5071.1	3170.0	1099.7
		16 S 32	30.0	0.2	15.9	6374.0	6033.1	3771.0	1061.9
		17 Cl 35	35.1	0.3	16.9	7465.0	7047.1	4405.0	1036.6
		18 Ar 40	42.0	0.3	17.9	8970.0	8417.1	5261.0	983.7
		19 K 39	45.3	0.3	18.9	9699.0	9141.1	5714.0	1020.9
	500	20 Ca 40	52.4	0.3	19.9	11259.0	10573.1	6609.0	990.1
		21 Sc 45	58.7	0.3	20.9	12645.0	11867.1	7418.0	985.1
		22 Ti 48	65.9	0.4	21.9	14259.0	13363.1	8353.0	973.6
		23 V 51	74.2	0.4	22.9	16124.0	15079.1	9425.0	957.7
		24 Cr 52	83.4	0.4	23.9	18201.0	16982.1	10615.0	941.6
		25 Mn 55	91.6	0.4	24.9	20076.0	18732.1	11708.0	941.7
		26 Fe 56	101.6	0.4	25.9	22380.0	20852.1	13034.0	931.9
		27 Co 59	111.8	0.5	26.9	24773.0	23063.1	14416.0	926.6
		28 Ni 58	125.5	0.5	28.0	27990.0	25972.1	16234.0	905.6
		29 Cu 63	138.0	0.5	29.0	30964.0	28701.1	17940.0	899.1
		30 Zn 64	152.1	0.5	30.0	34376.0	31814.1	19885.0	890.1
		31 Ga 69	166.6	0.5	31.0	37921.0	35064.1	21917.0	885.0
		32 Ge 74	182.6	0.5	32.0	41892.0	38694.1	24186.0	879.0
		33 As 75	200.3	0.6	33.0	46351.0	42756.1	26725.0	871.9
		34 Se 80	220.8	0.6	34.0	51599.0	47508.1	29695.0	862.1

		35 Br 79	242.5	0.6	35.0	57283.0	52661.1	32916.0	854.4
G-5	1000	8 O 16	1.4	0.1	6.6	298.0	292.0	183.0	3669.7
		9 F 19	2.1	0.1	7.7	441.0	430.8	269.0	3409.0
		10 Ne 20	3.1	0.1	8.9	657.0	638.7	399.0	3054.5
		11 Na 23	3.9	0.1	9.9	812.0	789.4	493.0	3062.0
		12 Mg 24	5.1	0.1	11.0	1071.0	1037.8	649.0	2878.1
		13 Al 27	6.6	0.1	12.1	1378.0	1330.7	832.0	2714.8
		14 Si 28	8.1	0.1	13.2	1701.0	1638.4	1024.0	2612.0
		15 P 31	9.9	0.1	14.2	2081.0	1998.5	1249.0	2504.5
		16 S 32	11.9	0.2	15.3	2507.0	2400.5	1500.0	2410.4
		17 Cl 35	13.9	0.2	16.3	2928.0	2799.1	1750.0	2362.6
		18 Ar 40	16.3	0.2	17.4	3437.0	3277.1	2048.0	2290.6
		19 K 39	17.7	0.2	18.3	3735.0	3570.1	2232.0	2359.2
		20 Ca 40	20.3	0.2	19.4	4283.0	4086.1	2554.0	2307.8
		21 Sc 45	22.6	0.2	20.4	4776.0	4555.1	2847.0	2301.8
		22 Ti 48	25.4	0.2	21.4	5380.0	5125.1	3203.0	2267.5
		23 V 51	29.1	0.2	22.5	6172.0	5860.1	3663.0	2191.8
		24 Cr 52	32.8	0.3	23.5	6969.0	6601.1	4126.0	2140.2
		25 Mn 55	36.0	0.3	24.5	7673.0	7265.1	4541.0	2129.9
		26 Fe 56	39.8	0.3	25.5	8488.0	8026.1	5017.0	2105.0
		27 Co 59	43.7	0.3	26.6	9342.0	8825.1	5516.0	2084.9
		28 Ni 58	48.5	0.3	27.6	10396.0	9798.1	6124.0	2041.5
		29 Cu 63	52.9	0.3	28.6	11360.0	10697.1	6686.0	2025.4
		30 Zn 64	58.0	0.3	29.6	12495.0	11745.1	7341.0	1995.9
		31 Ga 69	63.1	0.4	30.6	13624.0	12793.1	7996.0	1978.3
		32 Ge 74	68.2	0.4	31.6	14784.0	13871.1	8670.0	1966.1
		33 As 75	74.1	0.4	32.7	16103.0	15088.1	9431.0	1944.7
		34 Se 80	80.4	0.4	33.7	17527.0	16400.1	10251.0	1923.9
		35 Br 79	86.9	0.4	34.7	19013.0	17768.1	11106.0	1905.4
		36 Kr 84	96.0	0.4	35.7	21085.0	19631.1	12270.0	1853.9
		37 Rb 85	102.6	0.4	36.7	22620.0	21056.1	13161.0	1851.3
		38 Sr 88	109.9	0.4	37.7	24319.0	22623.1	14141.0	1843.2
		39 Y 89	118.7	0.5	38.7	26381.0	24500.1	15314.0	1821.7
		40 Zr 90	128.7	0.5	39.8	28757.0	26644.1	16654.0	1793.6
		41 Nb 93	136.5	0.5	40.8	30617.0	28376.1	17736.0	1796.9
		42 Mo 98	148.6	0.5	41.8	33537.0	30990.1	19370.0	1763.0
		43 Tc 97	159.4	0.5	42.8	36170.0	33381.1	20865.0	1749.0

		44 Ru 102	170.3	0.5	43.8	38854.0	35828.1	22394.0	1740.1
		45 Rh 103	185.4	0.6	44.8	42610.0	39164.1	24479.0	1706.7
		46 Pd 106	195.7	0.6	45.8	45184.0	41556.1	25975.0	1713.0
		47 Ag 107	209.4	0.6	46.8	48690.0	44729.1	27958.0	1701.6
		48 Cd 114	221.8	0.6	47.8	51882.0	47663.1	29792.0	1702.0
		49 In 115	238.3	0.6	48.8	56160.0	51511.1	32197.0	1686.5

4. Results and Discussions

4.1 Radial dose

A fundamental step in RDD calculations is to make sure that the integration limits of the total annular energy density of Eq. 6 at width $(r = 0.1\ (nm) \longrightarrow (r = R_{eff})(nm)$ will yield the ion's LET applied in all targets as illustrated in Fig. 1. The effective range, R_{eff} (the upper integration limit) was thus determined. Fig. 1 shows that LETs calculated by the present work are identical to the tabulated electronic LET_{SRIM} for the 20 groups of ions in all targets.

The ratio between the determined effective range, R_{eff} to the total range R of the secondary electrons, $\frac{R_{eff}}{R}$ for the different ions of different square relative velocity β^2 is given for all targets in Fig.2. As the ion velocity increased as R_{eff} decreased.

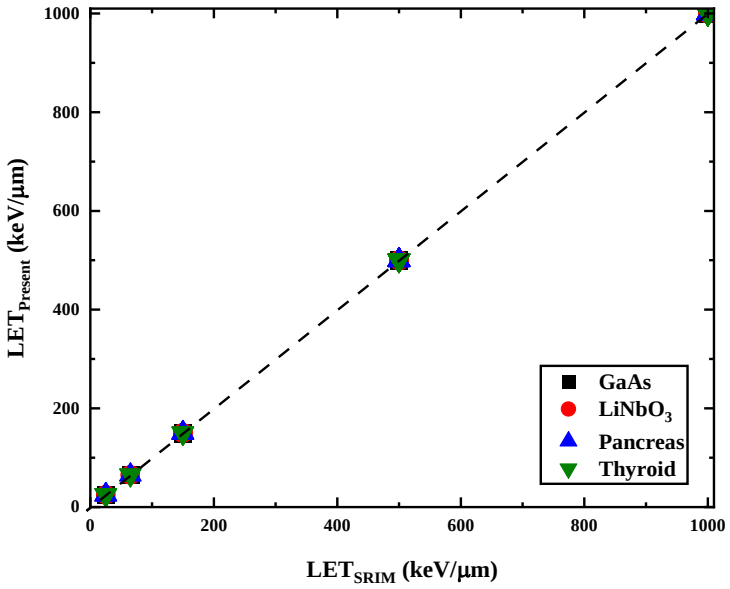

Fig. 1 The calculated $LET_{Present}$ versus tabulated LET_{SRIM} are almost identical for the 20 groups in all targets under investigation.

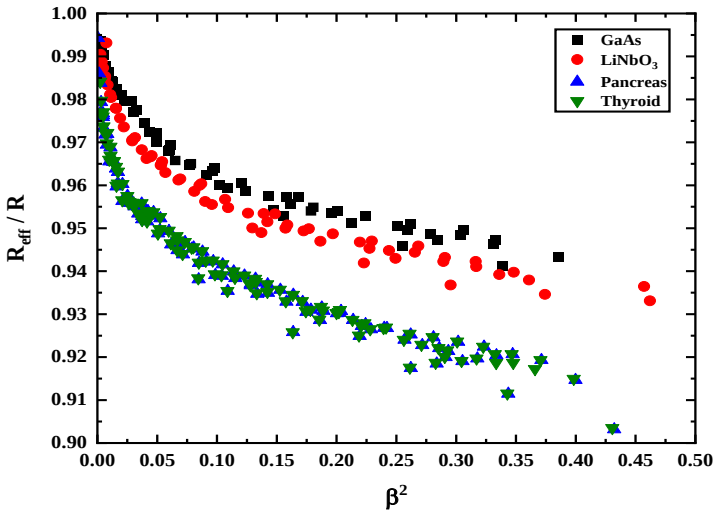

Fig. 2 The ratio between the effective range, R_{eff} to the total range R for the different ions in different targets of relative velocity β^2.

The radial dose distribution for the low energy 2 MeV/n p and C in Gallium arsenide (GaAs), Lithium Niobate ($LiNbO_3$), Pancreas and Thyroid, p and C in water is calculated by using the Butts-Katz range energy relation and compared with experimental and Geant-4 MC data are given in Fig.3 & Fig.4. The radial dose calculations for carbon in water agree with experimental data (Faïn et al., 1974) as well as Monte Carlo simulation (Incerti et al., 2014) and is given as an example.

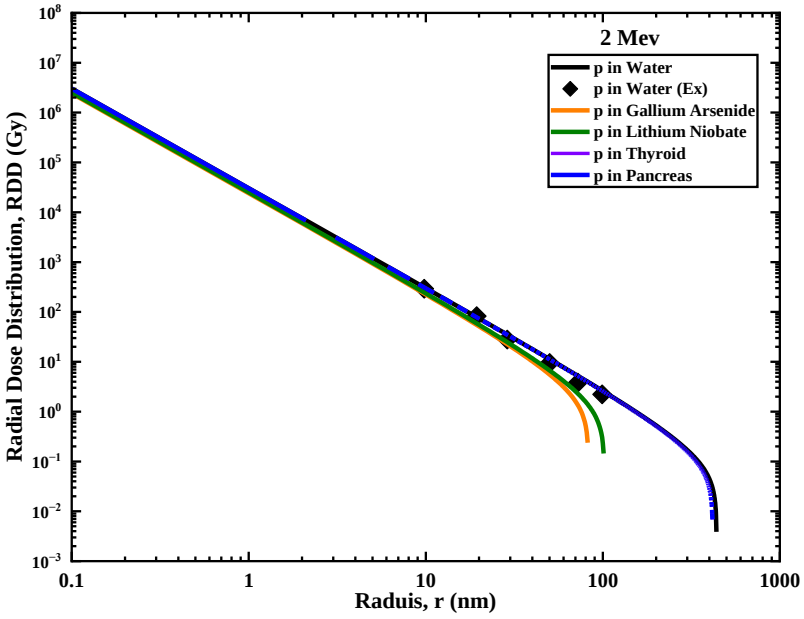

Fig. 3 Calculated radial dose for 2 MeV p in GaAs, $LiNbO_3$, Thyroid and Pancreas, and p in water is compared with experimental (Faïn et al., 1974).

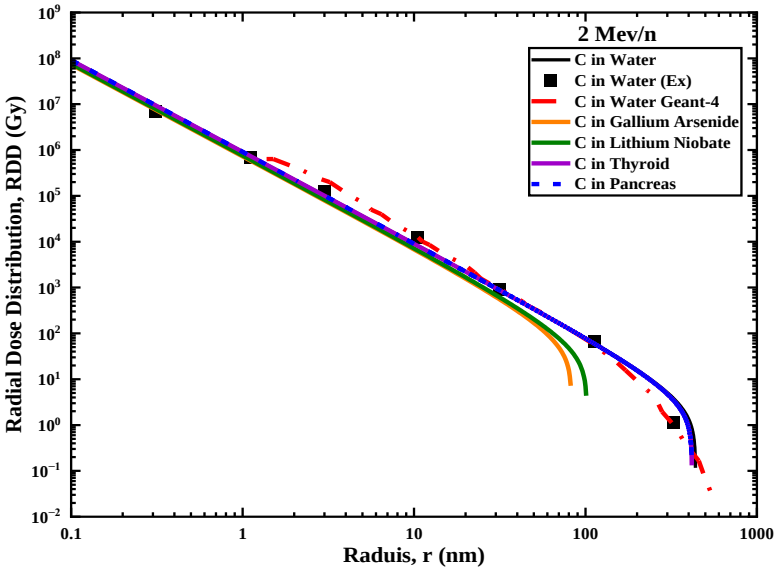

Fig. 4 Calculated radial dose for 2 MeV/n C in GaAs, $LiNbO_3$, Thyroid and Pancreas, and C in water is compared with experimental (Faïn et al., 1974) and Geant-4 MC data (Incerti et al., 2014).

4.2 Annular energy distribution, AED

The code written for Eq. 6 allows the estimation of annular energy distribution per nm, AED for any target at different annular energy widths, r_{AEW}. The AED, for each ion, first increases reaching maxima then declines as illustrated in Fig. 5a & Fig. 6a for GaAs (G-3) and Thyroid (G-3) targets, respectively. Even though these ions have the same LET, one can observe that annular energy growth with annular energy width shows different energy distribution with different energy rates (slopes) and wider distribution.

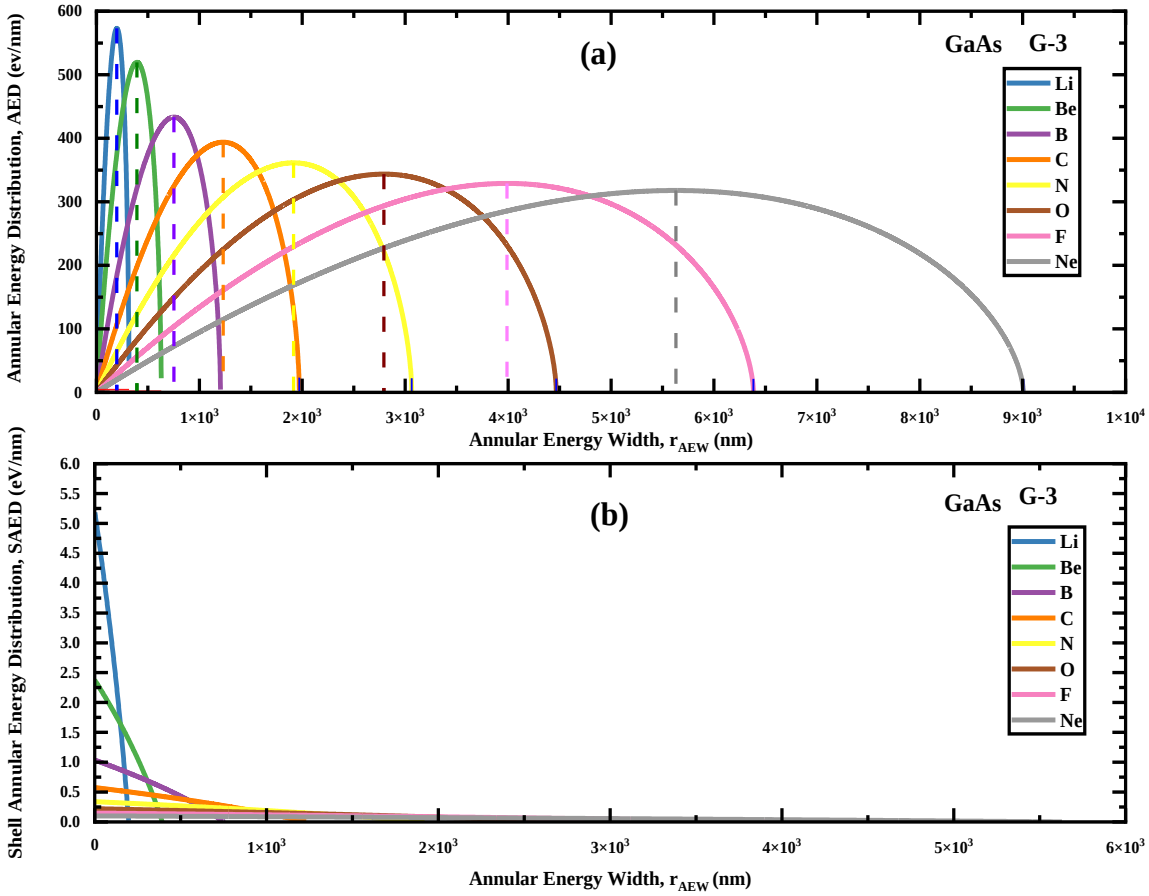

Fig. 5 a- Annular energy distribution, AED for GaAs (G-3) target as a function of the annular energy width, r_{AEW}. The ion's maximum annular energy width, r_{MAEW} for each ion is indicated by the dashed vertical lines. b- Shell annular energy distribution, SAED as a function of the annular energy width, r_{AEW} for GaAs (G-3) target as a function of the annular energy width, r_{AEW}.

The curves in these figures present a peak called the ion's maximum annular energy width, r_{MAEW}, and this width was determined for all groups and all targets. These growth rates are ion's β, Z^* dependence as will be shown later. Ion's maximum annular energy width was determined for the 337 ions in different targets. Annular energy (dose) distribution per nm is thus mapping the dose distribution around the ion and clearly shows the difference between ions of the same.

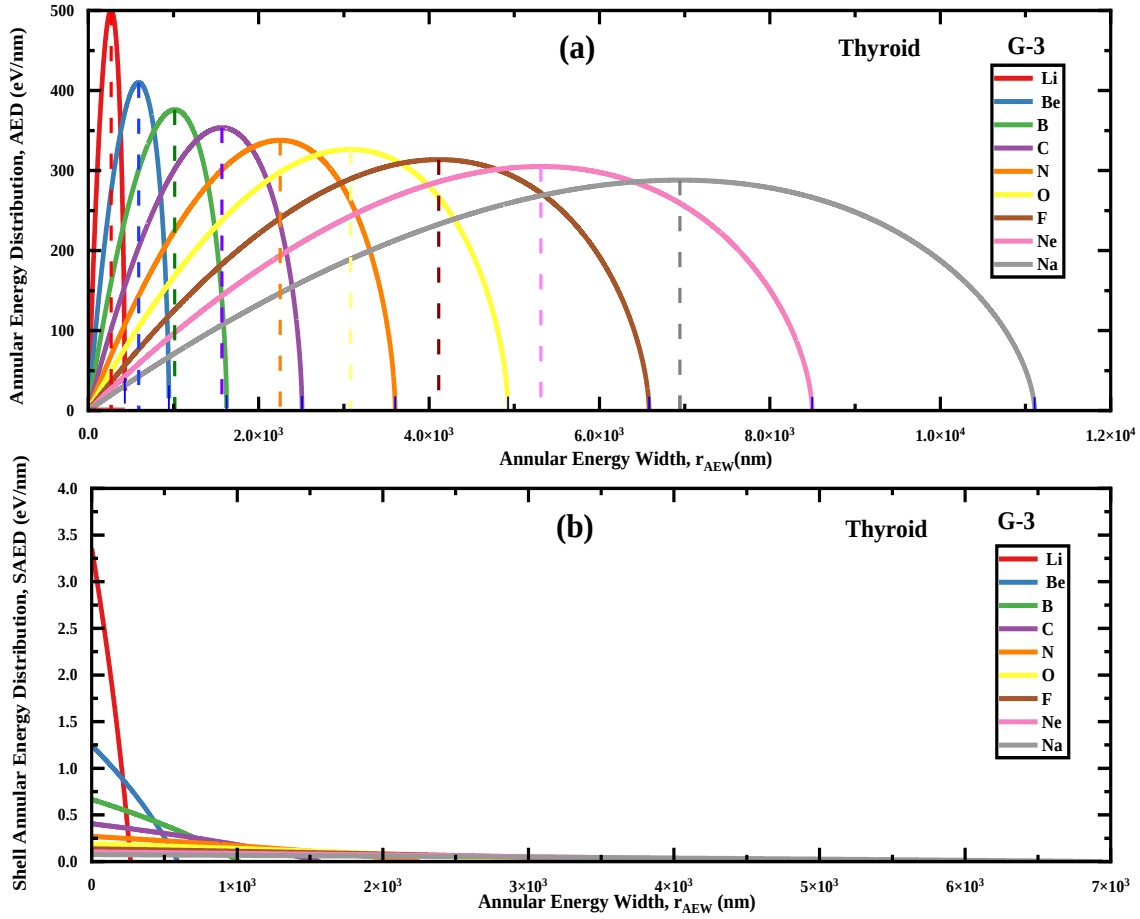

Fig. 6 a- Annular energy distribution, AED for Thyroid (G-3) target as a function of the annular energy width, r_{AEW}. The ion's maximum annular energy width, r_{MAEW} for each ion is indicated by the dashed vertical lines. b- Shell annular energy distribution, SAED as a function of the annular energy width, r_{AEW} for Thyroid (G-3) target as a function of the annular energy width, r_{AEW}.

4.3 Shell annular energy distribution, SAED

Shell annular energy distribution, SAED is the annular energy deposited in width equals 1 nm and is obtained by subtracting two successive annular energies of width 1 nm and 1nm apart.

The code written for Eq. 6 allows these calculations. Fig. 5b & Fig.6b present the SAED for ions of GaAs (G-3) and Thyroid (G-3) targets. One can observe the lower the ion energy, the larger the height of the shell's annular energy distribution, SAED, as expected. The higher the ion energy, the larger the annular energy width over which the energy is distributed. The energy distribution per nm decays drastically as a function of width with different rates, depending on the ion. Thus, the shell annular energy distributions for the different ions are not the same even though ions have the same LET (same group) for a variety of different targets. SAED reaches zero energy exactly at the so-called maximum annular energy width, r_{MAEW}. The r_{MAEW} for 337 ions of 20 groups was calculated to represent different targets either biological or used in industrial. The shell annular energy distribution is ion's β and Z^* dependent as will be explained later.

4.4 Maximum annular energy width study with ions and targets' parameters

The shell width at which the annular energy distribution per nm reaches its maximum is the radius at which the shell annular energy distribution becomes zero. This position is the r_{MAEW} and it is the key to understanding and applying the annular energy distribution concept in any application. The position r_{MAEW} was determined for the 337 ions covering an extended energy range (1-200 MeV/n) in various targets. This energy range covers many ion applications in medicine, industry, and space. The studied 337 ions give good statistics, deep learning, and more appliable process about this concept. The peak position is different for the different ions in the same group of the same LET as illustrated before.

The ratio of r_{MAEW} of the secondary electron to its effective range, R_{eff} for a given ion was determined as $\frac{r_{MAEW}}{R_{eff}}$. This ratio is surprisingly found at ≈ 63 % for the studied ions of all targets

under investigation as shown in Fig.7 with the ions β^2. Light ions with low energy of the studied 337 ions are showing a little increase or decrease in this ratio. r_{MAEW} showed a monotonic increasing function with the square of the ion's relative velocity, β^2 (Fig. 8) for all targets. As expected, the maximum annular energy width increases as the ion energy increases not all ion's energy was covered, therefore, the fitting equations were considered of r_{MAEW} with the ion's relative velocity β^2 give the expected r_{MAEW} for any ion's energy. Tables 5-6 show the polynomial fitting equation of r_{MAEW} with ions' β^2 for the different targets.

Table 5. The fitting parameters of the fitting equations of r_{MAEW}.

r_{MAEW} Polynomial Fitting Equations ($y = a + b_1x+b_2x^2$)		
Target	Constants	R^2
GaAs	a = 38.40005 b_1 =10107.63415 b_2 = 20430.46571	0.99973
$LiNbO_3$	a =101.96706 b_1 = 10859.37601 b_2 = 30535.57497	0.99901
Pancreas	a = 233.79385 b_1 = 48787.65444 b_2 = 104576.14612	0.99955
Thyroid	a = 255.79088 b_1 = 48581.20876 b_2 = 104935.46237	0.99961

Table 6. The fitting parameters of the fitting equations of TAED.

TAED Linear Fitting Equations (y = a + bx)		
Target	Constants	R^2
GaAs	a = 1.10731 b = 1.05126	1
$LiNbO_3$	a = 0.66751 b = 0.88397	1
Pancreas	a = 0.07354 b = 0.25929	1
Thyroid	a = 0.09123 b = 0.25879	1

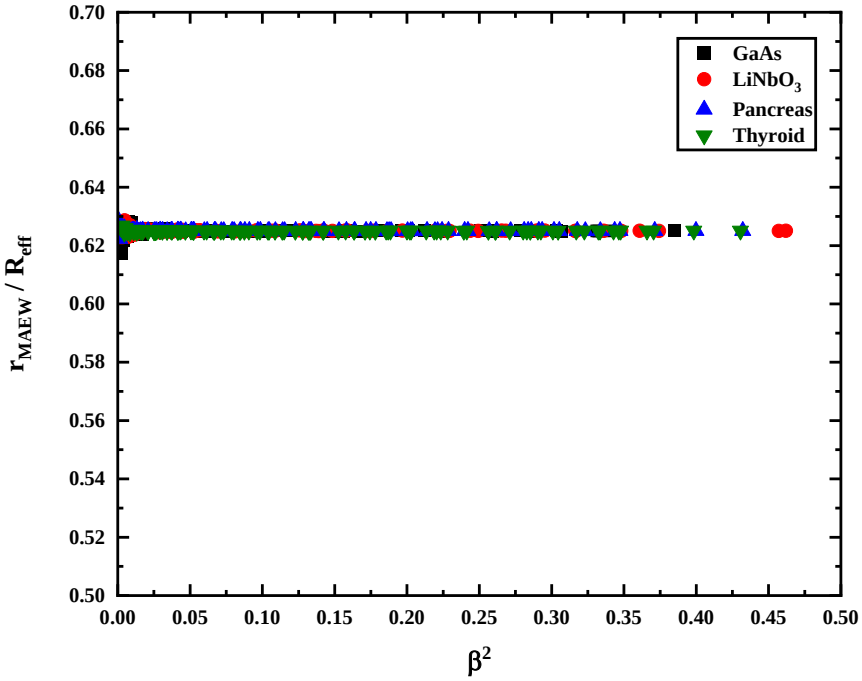

Fig. 7 The $\frac{r_{MAEW}}{R_{eff}}$ as a function of the ion β2 for the 337 ions. Light ions show a little increase or decrease in this ratio.

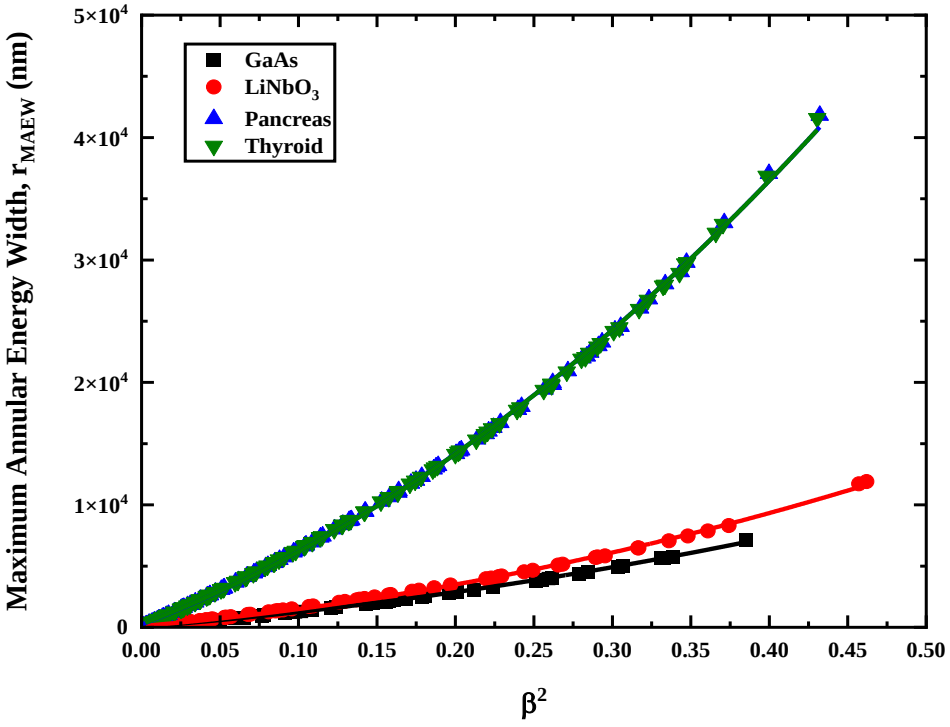

Fig. 8 Ion's maximum annular energy width, rMAEW, shows a monotonic increasing function with the square of the ion's relative velocity, β2 for all targets.

4.5 Total annular energy distribution study with ions and targets' parameters

The total annular energy distribution for different targets per nm, TAED, for the liberated secondary electrons is the energy delivered by the secondary electrons in the width between r = 0.1 (nm) and r = r_{MAEW} (nm). Thus, the integration limit of Eq. 6 can be adjusted accordingly.

TAED was calculated for 337 ions bombarded in different, and it shows linearly dependent on the ion's $(Z^*/\beta)^2$ as illustrated in Fig.9a & Fig.9b for compound and elements,

respectively. To deduce the total annular energy distribution for any ion at any $(Z^*/\beta)^2$ in the studied targets, a linear relation is deduced as given in Fig. 9 and Table 5 shows the linear fitting equations of TAED with ions $(Z^*/\beta)^2$ for the different targets.

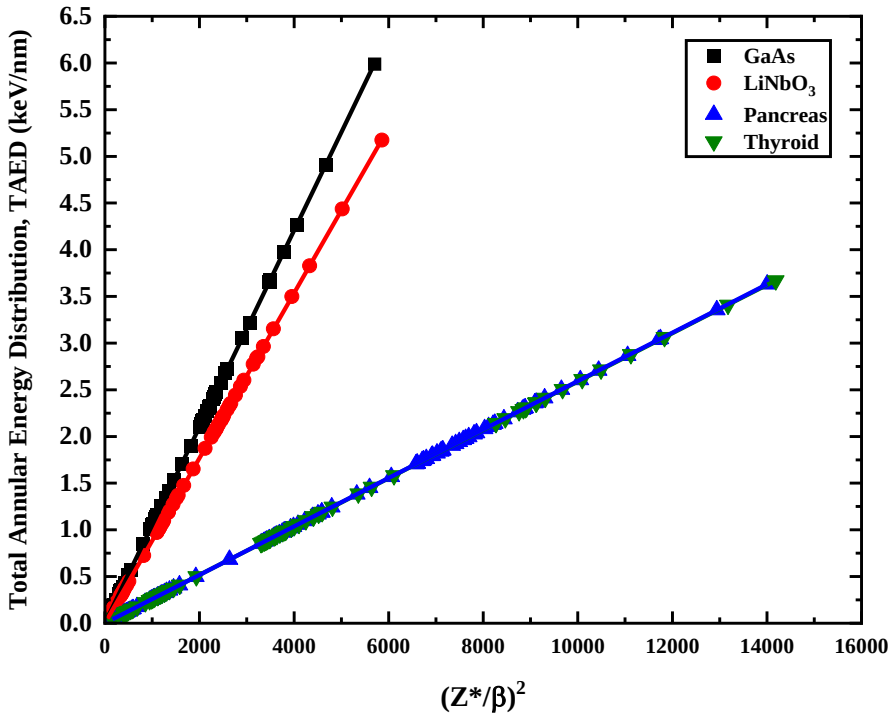

Fig. 9 Linear relations between the ion's total annular energy distribution, TAED, and (Z*/ β)2 for targets.

5. Conclusion

Annular energy distribution per nm, AED, is a new concept that can be used to estimate the energy deposited by any ion in any target. AED was calculated for a wide range of ions (337) of different energies (from 1 to 200 MeV/n) forming 20 different equal LET groups (from LET= 25 to LET=1000 keV/μm) in various targets. Based on Katz (radial dose distribution) and Butts-Katz R-E relation, the Annular energy distribution model was deduced. Even though equal LET ions can produce almost equal radial dose distribution, it has been found that energy distributions around the ions of the same LET are not the same in different compound targets. Annular energy distribution for equal LET ions shows different growing rates (slope) and wider distribution widths with different peak widths, r_{MAEW}.

Annular energy distribution, AED, variation with the annular width $r = 0.1\ (nm) \rightarrow r = R_{min}(nm)$ for the different ions shows a clear peak at a specific width. At this width, the shell annular energy distribution, SAED is found to drop to the zero-energy deposited for the distinct targets under investigation. This peak width for the 337 ions bombarded in different targets was determined.

The ratio of maximum annular energy width, r_{MAEW} of given ions to the corresponding effective range, R_{eff} was determined as $\frac{r_{MAEW}}{R_{eff}}$ and it was showing an almost equal ratio of ≈ 63% for all the studied ions in all studied targets.

The maximum annular energy width over which the energy is deposited is an ion as well as a target dependent. r_{MAEW} shows an increasing monotonic function of the square of the ion's relative velocity, β^2.

The total annular energy deposited by 337 ions bombarded in nine different targets was estimated. It was found that TAED shows a monotonic linear function with the ion $(Z^*/\beta)^2$. TAED is in $\frac{keV}{nm}$ order of magnitude. The TAED can be determined for all targets at any ions' $(Z^*/\beta)^2$.

Funding

The authors declare that no funds, grants, or other support were received during the preparation of this manuscript.

Competing Interests

The authors have no relevant financial or non-financial interests to disclose.

Availability of data and material

All data supporting this work are original and is included within the manuscript. The corresponding author is responsible for supplying any additional data.

References

Algora, C., Ortiz, E., Rey-Stolle, I., Díaz, V., Peña, R., Andreev, V.M., Khvostikov, V.P., Rumyantsev, V.D., (2001). A GaAs solar cell with an efficiency of 26.2% at 1000 suns and 25.0% at 2000 suns. IEEE Trans. Electron Devices 48, 840-844.

Awad, E.-S., Abu-Shady, M., Fromm, M., (2022). Distribution of radial dose in water at nanometer scale for ions of the same linear energy transfer: benefits of the concept of annular dose. Physica Scripta 97, 105003.

Awad, E.-S., Salah, A., Abu-Shady, M., Hassan, S., (2023). Annular energy and radial dose distributions study for a wide range of ions of different equal LET groups in water. Radiation Physics and Chemistry, 110771.

Awad, E.M., Abu-Shady, M., (2019). Inactivation cross section induced by heavy ions of different energies in Bacterial cells of E. coli: An analytical approach. Nuclear Instruments and Methods in Physics Research Section B: Beam Interactions with Materials and Atoms 457, 49-55.

Awad, E.M., Abu-Shady, M., (2020). Radial dose distribution and effective delta ray radius (Penumbra radius): Determination for some ions passing through water. Nuclear Instruments and Methods in Physics Research Section B: Beam Interactions with Materials and Atoms 462, 1-9.

Awad, E.M., El Masady, I., Rammah, Y.S., Abu-Shady, M., (2018). Simulating the radial dose distribution for charged particles in water medium by a semi-empirical model: An analytical approach. Applied Radiation and Isotopes 142, 135-142.

Bailey, S.G., Flood, D.J., (1998). Space photovoltaics. Progress in Photovoltaics: Research and Applications 6, 1-14.

Barkas, W.H., (1963). Nuclear Research Emulsions: techniques and theory. Academic Press.

Bazzan, M., Fontana, M., (2015). Preface to special topic: Lithium niobate properties and applications: reviews of emerging trends. AIP Publishing LLC, 040501.

Blakely, E.A., Ngo, F.Q.H., Curtis, S.B., Tobias, C.A., (1984). Heavy-Ion Radiobiology: Cellular Studies. Advances in Radiation Biology 11, 295-389.

Boorboor, S., Feghhi, S.A.H., Jafari, H., (2015). Investigation of radial dose effect on single event upset cross-section due to heavy ions using GEANT4. Radiation Measurements 78, 42-47.

Butts, J.J., Katz, R., (1967). Theory of RBE for heavy ion bombardment of dry enzymes and viruses. Radiat Res 30, 855-871.

Chatterjee, A., Schaefer, H.J., (1976). Microdosimetric structure of heavy ion tracks in tissue. Radiation and Environmental Biophysics 13, 215-227.

Cucinotta, F.A., Katz, R., Wilson, J.W., Dubey, R.R., (1996). Radial dose distributions in the delta-ray theory of track structure. AIP Conference Proceedings 362, 245-265.

Cucinotta, F.A., Nikjoo, H., Goodhead, D.T., (1999). Applications of amorphous track models in radiation biology. Radiation and Environmental Biophysics 38, 81-92.

Faïn, J., Monnin, M., Montret, M., (1974). Spatial Energy Distribution around Heavy-Ion Path. Radiation Research 57, 379-389.

Fromm, M., Abu-Shady, M., Groetz, J.E., Awad, E.M., (2021). Etched track profiles for relativistic 7 GeV silicon and 17.48 GeV Nickel ions in PADC detector: The case study of convex track walls. Radiation Physics and Chemistry 187, 109566.

Iles, P.A., (2000). Future of photovoltaics for space applications. Progress in Photovoltaics: Research and Applications 8, 39-51.

Incerti, S., Psaltaki, M., Gillet, P., Barberet, P., Bardiès, M., Bernal, M.A., Bordage, M.C., Breton, V., Davidkova, M., Delage, E., El Bitar, Z., Francis, Z., Guatelli, S., Ivanchenko, A., Ivanchenko, V., Karamitros, M., Lee, S.B., Maigne, L., Meylan, S., Murakami, K., Nieminen, P., Payno, H., Perrot, Y., Petrovic, I., Pham, Q.T., Ristic-Fira, A., Santin, G., Sasaki, T., Seznec, H., Shin, J.I., Stepan, V.,

Tran, H.N., Villagrasa, C., (2014). Simulating radial dose of ion tracks in liquid water simulated with Geant4-DNA: A comparative study. Nuclear Instruments and Methods in Physics Research Section B: Beam Interactions with Materials and Atoms 333, 92-98.

Katz, R., (1976). Track structure theory in radiobiology and in radiation detection. Nuclear Track Detection 2, 1-28.

Kiefer, J., (2008). The physical basis for the biological action of heavy ions. New Journal of Physics 10, 075004.

Kiefer, J., Straaten, H., (1986). A model of ion track structure based on classical collision dynamics (radiobiology application). Physics in Medicine and Biology 31, 1201-1209.

Kobetich, E.J., Katz, R., (1968). Energy Deposition by Electron Beams and $\ensuremath{\delta}$ Rays. Physical Review 170, 391-396.

Korcyl, M., (2014). Track structure modelling for ion radiotherapy. arXiv preprint arXiv:1410. 5250.

Malouff, T.D., Mahajan, A., Krishnan, S., Beltran, C., Seneviratne, D.S., Trifiletti, D.M., (2020). Carbon ion therapy: a modern review of an emerging technology. Frontiers in oncology 10, 82.

Nikjoo, H., Emfietzoglou, D., Liamsuwan, T., Taleei, R., Liljequist, D., Uehara, S., (2016). Radiation track, DNA damage and response—a review. Reports on Progress in Physics 79, 116601.

Nikjoo, H., Uehara, S., Emfietzoglou, D., Interaction of radiation with matter. CRC press.

Oda, N., Lyman, J.T., (2012). Secondary-Electron Distribution for Heavy Ions. Radiation Research Supplement 7, 20-32.

Snyder, C., (1997). National Aeronautics and Space Administration (NASA) NASA. Encyclopedia of Planetary Science: Springer.

Spohr, R., (1990). Ion Tracks and Microtechnology. Vieweg+Teubner Verlag Wiesbaden, Institut für Kernphysik, Johann Wolfgang Goethe-Universität, Frankfurt 90, Germany.

Staebler, D.L., Amodei, J.J., Thermally fixed holograms in linbo3. Ferroelectrics 3, (1972) 107-113.

Waligorski, M., Hamm, R., Katz, R., (1986). The radial distribution of dose around the path of a heavy ion in liquid water. International Journal of Radiation Applications and Instrumentation. Part D. Nuclear Tracks and Radiation Measurements 11, 309-319.

Waligórski, M.P.R., Grzanka, L., Korcyl, M., (2015). The principles of Katz's cellular track structure radiobiological model. Radiation Protection Dosimetry 166, 49-55.

Waligórski, M.P.R., Hamm, R.N., Katz, R., (1986). The radial distribution of dose around the path of a heavy ion in liquid water. International Journal of Radiation Applications and Instrumentation. Part D. Nuclear Tracks and Radiation Measurements 11, 309-319.

Wang, X., Dutt, S., Notthoff, C., Kiy, A., Mota-Santiago, P., Mudie, S.T., Toimil-Molares, M.E., Liu, F., Wang, Y., Kluth, P., (2022). SAXS data modelling for the characterisation of ion tracks in polymers. Physical Chemistry Chemical Physics 24, 9345-9359.

Weis, R.S., Gaylord, T.K.,. (1985). Lithium niobate: Summary of physical properties and crystal structure. Applied Physics A 37, 191-203.

Ziegler, J.F., Ziegler, M.D., Biersack, J.P., (2010). SRIM – The stopping and range of ions in matter (2010). Nuclear Instruments and Methods in Physics Research Section B: Beam Interactions with Materials and Atoms 268, 1818-1823.